Journal of King Saud University - Science 36 (2024) 103576

HOSTED BY

Contents lists available at ScienceDirect

Journal of King Saud University - Science

journal homepage: www.sciencedirect.com

Full Length Article

Comparative study of PS and PES and their sulfonated forms in antifouling behavior and rejection efficiency

Ibrahim Hotan Alsohaimi

Chemistry Department, College of Science, Jouf University, Sakaka P.O. Box 2014, Saudi Arabia

ARTICLE INFO

Keywords:
Polysulfone
Polyethersulfone
Sulfonation process
Permeability
Ultrafiltration
Antifouling
Rejection

ABSTRACT

In this study, novel hybrid ultrafiltration (UF) membranes were developed using polyethersulfone (PES), polysulfone (PS), and their sulfonated counterparts (SPES and SPS) to enhance water flux and antifouling properties. FTIR and XRD analyses validated the successful incorporation of sulfonate groups and structural changes, while SEM images revealed more porous and uniform membrane structures. Thermogravimetric analysis (TGA) showed enhanced thermal stability for the sulfonated membranes. Mechanical property evaluations demonstrated that the sulfonated membranes maintained good tensile strength and flexibility. Water uptake and porosity measurements indicated increased hydrophilicity and porosity for SPES and SPS membranes compared to their pristine forms. The pure water flux of SPES (130 L/m^2·h) is significantly higher compared to PES (110 L/m^2·h). The sulfonated membranes (SPS and SPES) exhibit significantly enhanced antifouling properties, as demonstrated by the improved flux recovery ratios (FRR) for SA, BSA, and HA compared to their non-sulfonated counterparts (PS and PES), reaching up to 75 % for SPES. The rejection performance for BSA, HA, and SA solutions showed that SPES membranes achieved 95 %, 90 %, and 92 % rejection rates, respectively, compared to 80 %, 75 %, and 70 % for PS membranes. Fouling resistance tests using BSA, HA, and SA solutions showed that SPES and SPS membranes had significantly higher flux and lower fouling tendencies.

1. Introduction

Water shortage is a critical global issue affecting billions of people worldwide, driven by population growth, climate change, overextraction of groundwater, pollution, and inefficient water management. The increasing demand for water strains existing supplies, especially in regions already facing scarcity (Baker, 2023; Mekonnen and Hoekstra, 2024). Membrane-based systems, such as nanofiltration, reverse osmosis, microfiltration, and ultrafiltration, are highly effective in removing a wide range of impurities, including salts, organic compounds, pathogens, and particulate matter(Dharupaneedi et al., 2019). The ultrafiltration process is a critical membrane-based separation technology for water purification and wastewater treatment. Materials commonly used in ultrafiltration membranes include polymers like PES (Alsohaimi et al., 2023), polyvinylidene fluoride (PVDF) (Aldawsari et al., 2022), and PS (Alshahrani et al., 2022), which offer superior chemical and thermal durability, and mechanical strength. Ultrafiltration is highly efficient in removing contaminants, energy-efficient, scalable, and resistant to various chemicals. It is a versatile and effective solution for producing clean water in various applications (Shi et al., 2014). PES is a high-performance polymer widely employed in ultrafiltration membranes for water purification and industrial applications due to its excellent mechanical strength, thermal stability, and chemical resistance. PES membranes face several challenges: (i) Fouling, which reduces performance and increases costs, can be mitigated by surface modifications like hydrophilic polymer grafting. (ii) PES's hydrophobic nature leads to lower water flux and higher fouling, which can be addressed by blending with hydrophilic polymers or applying coatings. (iii) Mechanical stability is compromised under repeated stress and pressure fluctuations. Designing robust support structures and optimizing module configurations can enhance stability and longevity (Celik Madenli et al., 2021; Guo and Kim, 2017; Kheirieh et al., 2018; Kochkodan et al., 2008; Ma et al., 2007; Serbanescu et al., 2020; Shannon et al., 2008; Shen et al., 2011; V. B. et al., 2020; Venault et al., 2017; Wang et al., 2020, 2019; Yi et al., 2012; Zhang et al., 2018). One effective method to mitigate fouling in PES and PS membranes is through sulfonation. Sulfonation introduces hydrophilic sulfonic acid ($-SO_3H$) groups onto the polymer, boosting hydrophilicity and reducing fouling. This process enhances membrane performance by increasing water affinity, ion exchange capacity, and permeability while lowering

E-mail address: ehalshaimi@ju.edu.sa.

https://doi.org/10.1016/j.jksus.2024.103576
Received 2 September 2024; Received in revised form 23 November 2024; Accepted 29 November 2024
Available online 30 November 2024

water contact angles. These changes result in a more interconnected porous structure, improved antifouling properties, and greater water uptake, making sulfonated membranes ideal for water purification and gas separation applications (Sadare and Daramola, 2021; Van der Bruggen, 2009; Zhao et al., 2013).

In this work, I fabricated a membrane by introducing PS, PES, and their sulfonated forms to enhance antifouling behavior and rejection efficiency. The integration of PS, PES, and their sulfonated variants seeks to boost the permeability and antifouling features by utilizing the excellent surface energy of the sulfonated products. These fabricated polymer membranes were assessed for antifouling tests through measurements of water flux, sodium alginate (SA), humic acid (HA), and bovine serum albumin (BSA).

2. Materials and methods

Detailed information on the materials used in this work is provided in the Supporting Information.

2.1. Membrane fabrication

UF membrane preparation procedure utilized the Non-Solvent Induced Phase Separation (NIPS) method, as described in previous publications by the same research group [9–11]. In this process, 18 wt% of PES, PS, SPES, or SPS, along with 2 wt% polyvinylpyrrolidone (PVP), were gradually added to N-methyl-2-pyrrolidone (NMP) while stirring at 350 rpm at 40 °C for 3 h. The mixture was sonicated for 60 min to form a homogeneous suspension, stirred for 24 h, sonicated again, and allowed to rest to eliminate air bubbles. The casting solution was spread onto a clean glass plate to a thickness of 200 μm. After a 20-second air-drying period, the membrane was immersed in a water bath and rinsed with deionized water to remove residual solvent. The membranes were labeled PES, SPES, PS, and SPS.

2.2. Permeability and antifouling performance

The permeability and UF performance of the synthesized membranes were assessed using a stirred dead-end UF cell (Amicon-8050). Detailed information on the antifouling variables is provided in the Supporting Information (**S5**).

3. Results and discussion

3.1. Characterization of the fabricated membrane

The ATR-FTIR spectra of PES, PS, and their sulfonated products (SPES and SPS) are depicted in Fig. 1**(a)**. The FTIR spectrum of PS reveals characteristic peaks, such as a broad O–H stretching vibration at 3350 cm^{-1} (Alosaimi et al., 2022; El-Sayed et al., 2023) and C–H stretching at 2966 cm^{-1}. Peaks at 1583 cm^{-1} and 1486 cm^{-1} indicate C = C stretching in aromatic rings, while asymmetric and symmetric C–H bending vibrations are observed at 1406 cm^{-1} and 1368 cm^{-1}, respectively. Other notable peaks include C = C stretching at 1323 cm^{-1}, S = O asymmetric stretching at 1289 cm^{-1}, and C-O-C stretching at 1236 cm^{-1} and 1102 cm^{-1}. The S = O symmetric stretching at 1149 cm^{-1} and C–H bending at 832 cm^{-1} further characterize PS. For PES, the FTIR spectrum shows O–H stretching at 3350 cm^{-1} and C = C stretching at 1583 cm^{-1} and 1486 cm^{-1}, similar to PS. However, PES presents distinct peaks at 1402 cm^{-1} for asymmetric C–H bending and a strong S = O symmetric stretching band at 1139 cm^{-1}, indicating the presence of sulfone groups. Additionally, C-O-C stretching is observed at 1100 cm^{-1}, highlighting the ether linkages in PES. These spectral differences demonstrate the structural variations and functional group presence between PS and PES, emphasizing the sulfone and ether groups in PES that are less prominent in PS (Mannan et al., 2015). Upon sulfonation, less notable changes in the FTIR spectra of SPES and SPS are observed. The similarity in FTIR spectra before and after modification might occur because the functional groups introduced during modification, such as sulfonation, do not produce significant shifts in the overall absorption bands. This means that the main backbone structure of the polymers (PS and PES) remains unchanged, with only slight changes observed for specific functional groups.

The XRD patterns of pristine PES, PS, and their sulfonated products (SPES and SPS) are presented in Fig. 1**(b)**. The XRD pattern of PES exhibits a broad peak centered around 2θ = 18°, which is indicative of its amorphous nature. This broad peak suggests that PES lacks a long-range crystalline order. Similarly, the XRD pattern of PS depicts a broad peak around 2θ = 20°, also indicative of its amorphous structure. The absence of sharp diffraction peaks in PES and PS confirms their non-crystalline nature. Upon sulfonation, the XRD patterns of SPES and SPS display significant changes. For SPES, the broad peak around 2θ = 18° becomes more intense and slightly shifts, suggesting some degree of structural reorganization and potential partial crystallinity induced by the presence of sulfonic acid groups. In SPS, the broad peak around 2θ = 20° also shows an increase in intensity, indicating similar structural modifications due to sulfonation. These XRD results align with the FTIR findings, which confirm the successful introduction of sulfonic acid groups into the polymer matrix.

The Thermogravimetric Analysis (TGA) profiles of pristine PS, SPS, and SPES membranes are depicted in Fig. 2. The TGA plots provide insights into these membranes' thermal stability and decomposition behavior. The TGA profile of pristine PS shows a gradual weight-loss up

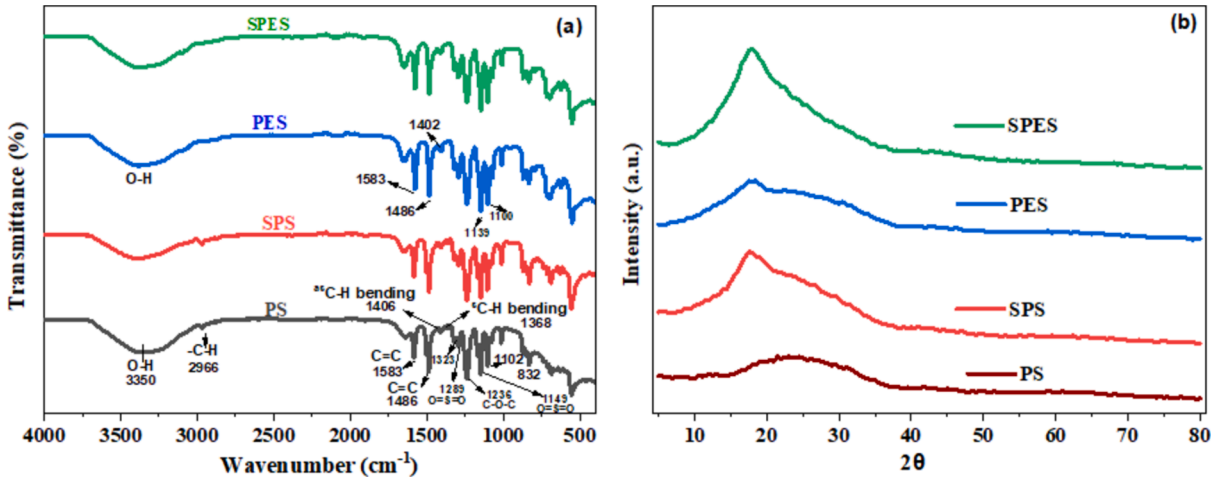

Fig. 1. (a) ATR-FTIR spectra, and (b) XRD patterns of pristine PES, PS and their sulfonation products (SPES and SPS) membranes.

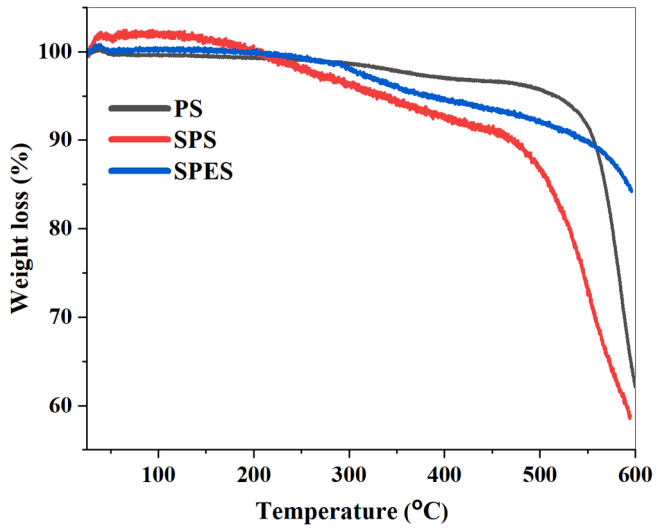

Fig. 2. TGA profiles of pristine PS, SPS and SPES membranes.

to around 500 °C, after which a sharp decline is observed. The initial weight loss up to 100 °C is minimal, indicating the loss of adsorbed moisture. The significant weight loss occurs between 400 °C and 500 °C, which can be related to the thermal degradation of the PS polymer backbone. The onset of significant decomposition starts at approximately 420 °C, and the maximum decomposition rate is observed around 480 °C. The TGA curve for SPS displays a different thermal behavior compared to pristine PS. The initial weight loss up to 100 °C is again minimal, primarily due to moisture loss. However, the onset of significant decomposition for SPS starts earlier, around 350 °C. This earlier decomposition onset can be attributed to the presence of sulfonic acid moieties, which decrease the thermal stability of the polymer. The significant weight loss occurs between 350 °C and 500 °C, with the maximum decomposition rate observed around 450 °C. This indicates that sulfonation reduces the thermal stability of PS. The TGA profile for SPES shows a similar trend to SPS, with some differences in the thermal degradation pattern. The initial weight loss due to moisture is minimal. The onset of significant decomposition for SPES is observed around 360 °C, slightly higher than SPS but still lower than pristine PS. The significant weight loss occurs between 360 °C and 520 °C, with the maximum decomposition rate around 470 °C. The presence of sulfonic acid groups in SPES also reduces the thermal stability compared to the pristine PES. The TGA analysis reveals that sulfonation impacts the thermal stability of both PS and PES (Liu et al., 2010; Wu et al., 2006). The pristine PS offers the highest thermal durability among the three, with significant weight loss only starting around 420 °C. Sulfonation introduces sulfonic acid groups into the polymer matrix, which act as sites for thermal degradation, thereby reducing the overall thermal stability. The reduction in thermal stability upon sulfonation is consistent with the structure of the sulfonated polymers (Liu et al., 2010; Wu et al., 2006).

The Scanning Electron Microscopy (SEM) images in Fig. 3 provide a detailed examination of the top surface and cross-sectional morphology of PES, PS, and their sulfonated counterparts (SPES and SPS) membranes. The top surface images for all membranes (PS, SPS, PES, and SPES) exhibit smooth surfaces without visible pores, indicating a dense top layer structure typical of NIPS membranes. The PS membranes (Fig. 3 **a**) display a smooth top surface with no visible pores, and the cross-sectional images reveal an asymmetric structure characterized by a dense top layer and a sublayer with finger-like pores. This morphology

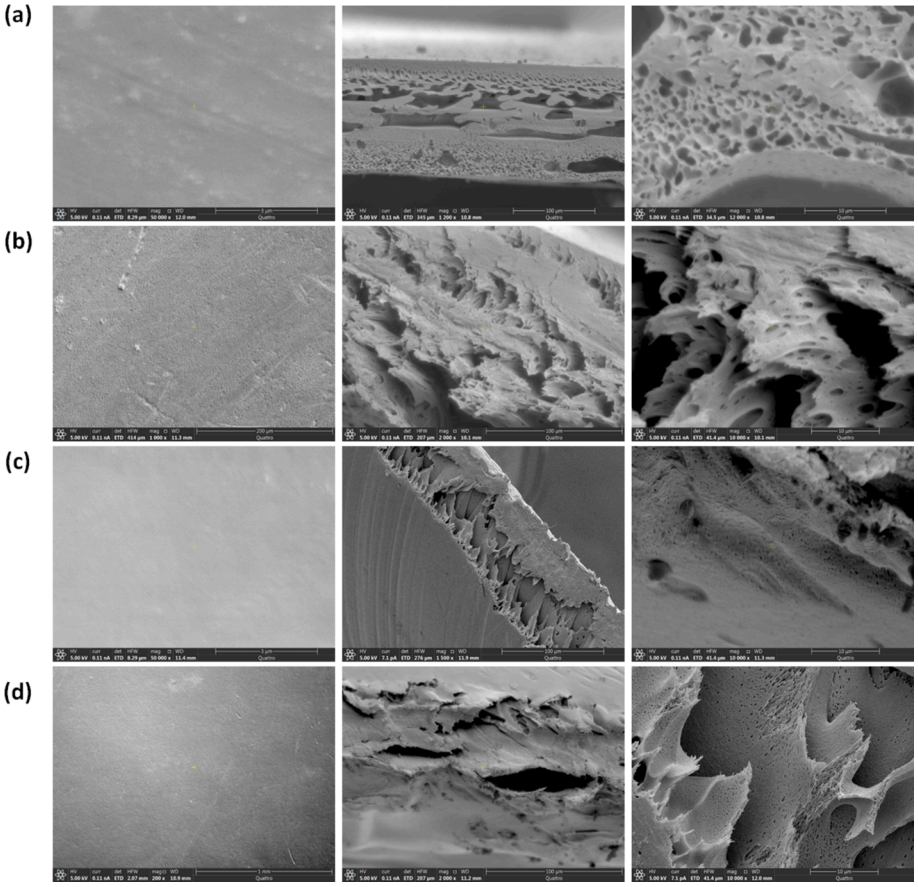

Fig. 3. The topography (Left) and cross-sectional (Middel and Right) SEM images of (a) PS, (b) SPS, (c) PES, and (d) SPES membranes.

aligns with the characteristics expected from a NIPS process. For the SPS membranes (Fig. 3**b**), the top surface remains smooth, while the cross-sectional images show a more pronounced finger-like pore structure compared to the neat PS membrane. The sulfonation of PS likely enhances the hydrophilicity of the membrane, facilitating a faster solvent/non-solvent exchange rate during phase separation, resulting in a more defined porous sublayer. The PES membranes (Fig. 3**c**) also show smooth top surfaces with non-visible pores. The cross-sectional images reveal an asymmetric structure with a dense top layer and a sublayer featuring broader and more extended finger-like pores compared to the PS membranes. This broader finger-like pore structure in PES membranes suggests a more efficient phase separation process, potentially due to the inherent properties of PES. For the SPES membranes (Fig. 3**d**), the top surface remains smooth without visible pores, similar to the other membranes. The cross-sectional images indicate a dense top layer with a sublayer having even more pronounced and extensive finger-like pores compared to the PES membrane. The presence of sulfonic acid groups in SPES enhances its hydrophilicity, accelerating the solvent/non-solvent exchange rate during membrane formation, which results in a more open and porous structure in the sublayer. The SEM analysis demonstrates that sulfonation significantly influences the morphology of the membranes, with both SPES and SPS exhibiting more defined and extensive finger-like pore structures in the sublayer compared to their non-sulfonated counterparts (PES and PS) (Rahimpour et al., 2010). This enhancement in pore structure is attributed to the increased hydrophilicity due to sulfonation, which facilitates a faster phase separation process.

The tensile stress–strain analysis of neat PES, PS, and their sulfonated products (SPES and SPS) membranes reveals significant insights into their mechanical properties (Fig. 4). Neat PES exhibits a high maximum stress of approximately 4.5 MPa and a moderate strain at break around 0.12 mm/mm, indicating good mechanical strength and elasticity. Neat PS, while slightly lower in maximum stress at about 4.2 MPa, shows greater elasticity with a strain at break of approximately 0.3 mm/mm. Upon sulfonation, both SPES and SPS display reduced mechanical properties. SPES shows a maximum stress of around 3.2 MPa and a strain at break of 0.1 mm/mm, while SPS exhibits a maximum stress of about 3.5 MPa and a strain at break of 0.15 mm/mm. The insertion of sulfonic acid moieties disrupts the polymer framework, reducing both tensile strength and elasticity(Fang et al., 2017). However, the trade-off includes enhanced hydrophilicity and antifouling behavior, which are crucial for membrane applications in water treatment. Despite the decrease in mechanical robustness, SPES and SPS membranes offer significant advantages in surface properties, making them suitable for applications requiring improved hydrophilicity and antifouling, thereby guiding the optimization of membrane materials for diverse industrial uses. The data presented in Fig. 5 highlights critical aspects of the membrane properties, specifically focusing on water uptake, porosity, contact angle, and surface free energy of the pristine and sulfonated PES and PS membranes. The pore size and distribution play a critical role in determining the overall performance of sulfonated membranes. The sulfonation process typically leads to changes in pore size due to the introduction of hydrophilic sulfonic acid groups, which can modify the interaction between the polymer chains and solvent during membrane fabrication. This results in an increase in pore size and improved uniformity in distribution. Larger and well-distributed pores enhance water permeability and reduce resistance to flow, contributing to higher flux values. Additionally, the increased hydrophilicity of the sulfonated membrane surfaces helps prevent pore blockage, improving antifouling properties. In Fig. 5**(a)**, the water uptake and porosity percentages are compared across the PS, SPS, PES, and SPES membranes. It is evident that the water uptake increases from PS to SPS and from PES to SPES, with the sulfonated membranes (SPS and SPES) showing significantly higher water uptake compared to their non-sulfonated counterparts. This increase in water uptake due to the hydrophilic nature of the SO_3H moieties introduced during the sulfonation process, which enhances the membranes' ability to absorb water. Similarly, the porosity of the membranes also follows an upward trend, with SPES exhibiting the highest porosity. The role of PVP as a pore-forming agent is crucial during membrane fabrication. When incorporated into the polymer

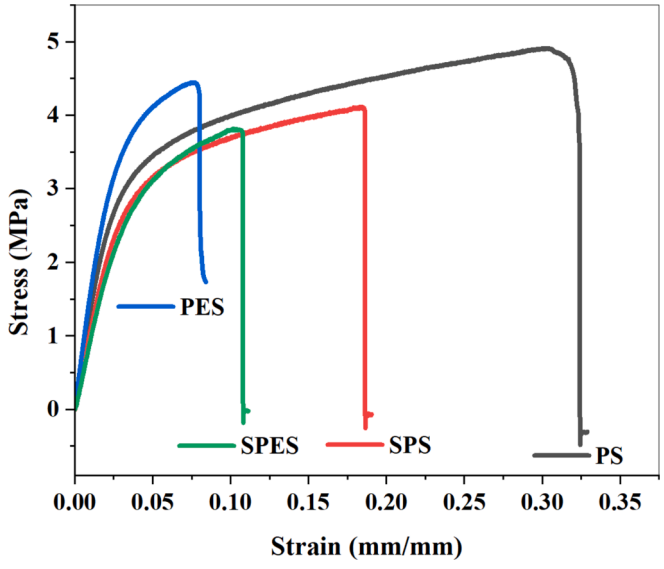

Fig. 4. The mechanical strength graphs for the pristine PES, PS and their sulfonation products (SPES and SPS) membranes.

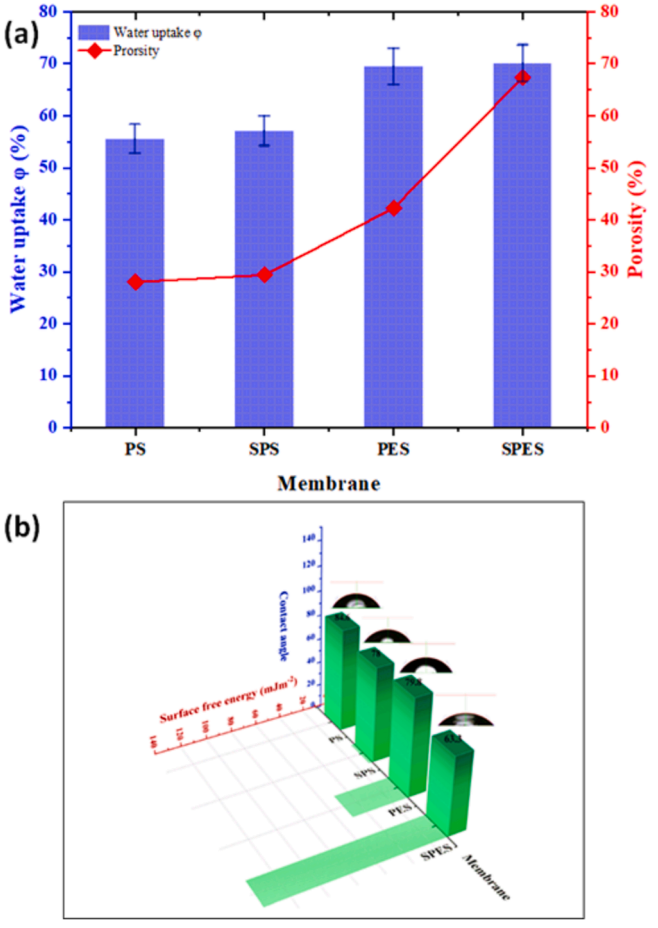

Fig. 5. (a) Porosity (%) as well as water uptake and (b) Contact angle and surface free energy of the pristine PES, PS and their sulfonation products (SPES and SPS) membranes.

matrix, PVP disrupts the uniform structure, leading to the formation of voids and enhanced porosity. During the phase inversion process, PVP dissolves, leaving behind pores that contribute to a highly interconnected porous network (Al Malek et al., 2012; Ho and Su, 2022). The enhanced porosity in sulfonated membranes is consistent with the SEM observations that revealed more pronounced and extensive finger-like pore structures, facilitating higher water uptake and increased permeability(Pereira et al., 2015). Fig. 5**(b)** illustrates the water contact angle and surface free energy of the same set of membranes. The PS membrane shows the highest contact angle (84.6°), indicating a more hydrophobic surface with lower surface free energy. Conversely, SPES exhibits the lowest contact angle (63.3°), suggesting a significant enhancement in hydrophilicity and surface energy compared to other membranes. The decrease in the contact angle from PES (79.8°) to SPES (63.3°) can be primarily attributed to the sulfonation process, which introduces more hydrophilic functional groups ($-SO_3H$) on the membrane surface. The reduced contact angles in SPES and SPS are indicative of enhanced surface wettability, which is crucial for antifouling properties. The difference in water contact angles between PES (79°) and SPES (63°) indicates an increase in surface hydrophilicity due to sulfonation. However, the water uptake values in Fig. 5**(a)** may not show a significant difference because water uptake is influenced by the overall porosity and internal structure of the membrane, not just surface properties. The sulfonic acid groups in SPES primarily enhance surface hydrophilicity without drastically altering the bulk porosity or internal water absorption capacity, resulting in minimal change in water uptake values. Additionally, the surface free energy values increase from PS to SPS and from PES to SPES, correlating with the higher hydrophilicity imparted by the sulfonation process. The increased surface free energy contributes to the improved linking between the surface of the membrane and water molecules, facilitating better water flow and reducing fouling tendencies (Khorsand-Ghayeni et al., 2017).

3.2. Membrane flux and antifouling assessment

3.2.1. Membrane flux

The data illustrated in Fig. 6 illustrate the influence of sulfonation on the pure water flux and the flux of foulants (BSA, HA, and SA) through the membranes. Fig. 6**(a)** shows the pure water flux (Jw) for PS, SPS, PES, and SPES membranes, while Fig. 6**(b)** displays the flux of foulant solutions through the same set of membranes. In Fig. 6**(a)**, it is evident that the pure water flux rises from PS to SPS and from PES to SPES. Specifically, the pure water flux for PS is around 100 L/m^2·h, while SPS shows an increased flux of approximately 120 L/m^2·h. For PES, the pure water flux is around 110 L/m^2·h, which further increases to about 130 L/m^2·h for SPES. This enhancement in water flux can be due to the boosted hydrophilicity and porosity of the sulfonated membranes (SPS and SPES), as previously discussed (Aldawsari et al., 2022; Alshahrani et al., 2022; Alsohaimi et al., 2023). The sulfonation process introduces hydrophilic sulfonic acid groups, which improve water uptake and surface wettability, as evidenced by the lower contact angles and higher surface free energy values. Fig. 6**(b)** presents the flux values for foulant solutions of BSA, HA, and SA through the membranes. For PS, the fluxes are approximately 30 L/m^2·h for BSA, 50 L/m^2·h for HA, and 70 L/m^2·h for SA. In comparison, SPS shows improved fluxes of around 50 L/m^2·h for BSA, 70 L/m^2·h for HA, and 90 L/m^2·h for SA. Similarly, PES exhibits fluxes of about 40 L/m^2·h for BSA, 60 L/m^2·h for HA, and 80 L/m^2·h for SA, which increase to approximately 60 L/m^2·h for BSA, 80 L/m^2·h for HA, and 100 L/m^2·h for SA in the SPES membranes. Variations in flux for BSA, HA, and SA are due to differences in molecular weight, structure, and charge. BSA's high molecular weight causes pore blocking and adsorption, reducing flux. HA forms a dense fouling layer, further lowering flux. SA creates a gel-like layer that blocks pores and increases resistance to flow, leading to flux variations (Myat et al., 2014; Zhao et al., 2015). Additionally, the enhanced flux values for the sulfonated membranes can be correlated with their increased hydrophilicity and porosity, which facilitate better water and foulant permeation. The higher porosity of the sulfonated membranes, as shown in Fig. 5**(a)**, also contributes to the increased flux by providing more pathways for water and foulant molecules to pass through.

3.2.2. Antifouling assessment

The Flux Recovery Ratio (FRR) of the bare PES, PS, and their sulfonated products (SPES and SPS) membranes for the foulants SA, BSA, and HA is depicted in Fig. 7. This figure highlights the membranes' ability to recover their flux after fouling, a critical parameter for assessing antifouling performance (Zhang et al., 2021). The FRR values for PS membranes show lower recovery, with FRR values around 45 %, 40 %, and 50 % for SA, BSA, and HA, respectively. Sulfonation of PS to SPS significantly enhances the FRR, with values increasing to approximately 60 %, 55 %, and 65 % for SA, BSA, and HA, respectively. Similarly, PES membranes exhibit FRR values of around 55 %, 50 %, and 60 % for SA, BSA, and HA, respectively. Upon sulfonation to SPES, the FRR values further improve to approximately 70 %, 65 %, and 75 % for SA, BSA, and HA, respectively. The enhanced FRR in sulfonated membranes (SPS and SPES) indicates a superior antifouling property compared to their non-sulfonated counterparts (PS and PES). The increased hydrophilicity and higher surface free energy of the sulfonated membranes, as observed

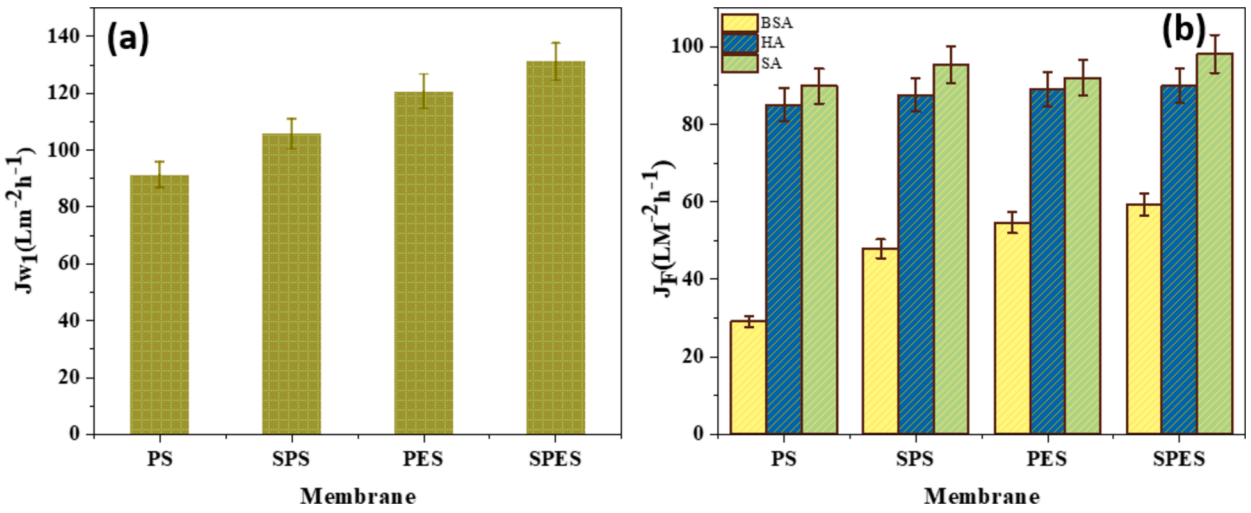

Fig. 6. (a) Water flux and (b) (HA, SA, and BSA) foulants solution flux performed at 1 bar of the neat PES, PS and their sulfonation products (SPES and SPS) membranes.

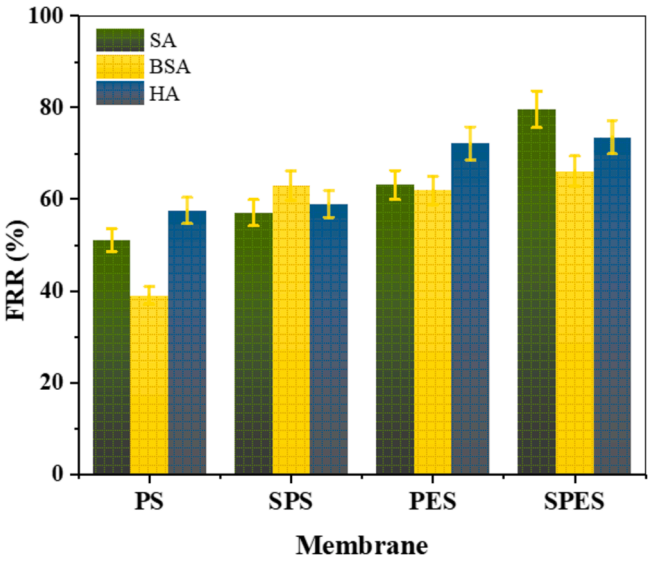

Fig. 7. Flux recovery ratio (FRR) of the bare PES, PS and their sulfonation products (SPES and SPS) membranes.

from the contact angle measurements and surface energy analysis, contribute to this improvement. These properties facilitate easier removal of foulants from the membrane surface, leading to better flux recovery. Additionally, the enhanced porosity of the sulfonated membranes, as indicated by the water uptake and porosity measurements, aids in maintaining higher flux after fouling.

Fig. 8 presents the fouling resistance (Rr and Rir) of the neat PES, PS, and their sulfonated products (SPES and SPS) membranes during the ultrafiltration (UF) of different foulants: (a) BSA, (b) HA, and (c) SA. The reversible resistance (Rr) and irreversible resistance (Rir) provide insight into the fouling behavior and cleaning efficiency of the membranes. For BSA (Fig. 8**a**), the PS membrane exhibits the lowest Rr (~5%) and the highest Rir (~60 %), indicating substantial fouling that is difficult to clean. Sulfonation of PS to SPS significantly increases the Rr to ~ 10 %, while decreasing the Rir to ~ 40 %, suggesting better cleanability. The PES membrane shows an Rr of ~ 15 % and an Rir of ~ 40 %, indicating improved fouling resistance compared to PS. Sulfonation to SPES further enhances the performance, with the highest Rr (~20 %) and lowest Rir (~35 %), reflecting the superior antifouling properties and easier cleaning of the SPES membrane. For HA (Fig. 8**b**), the PS membrane shows an Rr of ~ 25 % and a Rir of ~ 40 %. The SPS membrane improves the Rr to ~ 20 % and reduces the Rir to ~ 35 %. The PES membrane demonstrates an Rr of ~ 25 % and an Rir of ~ 38 %, while the SPES membrane exhibits the highest Rr (~30 %) and the lowest Rir (~32 %). This indicates that sulfonation significantly enhances the antifouling properties and cleanability of the membranes, especially for SPES. For SA (Fig. 8**c**), the PS membrane has an Rr of ~ 2 % and a Rir of ~ 45 %, indicating severe fouling. The SPS membrane shows a marked improvement with an Rr of ~ 4 % and an Rir of ~ 38 %. The PES membrane has an Rr of ~ 5 % and an Rir of ~ 35 %, while the SPES membrane exhibits the highest Rr (~6%) and the lowest Rir (~30 %), demonstrating excellent antifouling properties and ease of cleaning.

Fig. 9 illustrates the rejection assessment and adsorbed quantity of the neat PES, PS, and their sulfonated products (SPES and SPS) during UF of different foulants: (a) BSA, (b) HA, and (c) SA. The rejection percentage indicates the membrane's ability to retain foulants, while the adsorbed amount provides insight into the extent of fouling on the membrane surface. In Fig. 9**a**, for BSA, the neat PS membrane shows a rejection of ~ 70 % and an adsorbed amount of ~ 92 μg/cm^2, indicating significant fouling. The sulfonation of PS to SPS slightly improves the rejection to ~ 75 %, while the adsorbed amount remains nearly the same. The PES membrane demonstrates a rejection of ~ 80 % and a lower adsorbed amount of ~ 88 μg/cm^2, indicating better antifouling properties. The SPES membrane exhibits the highest rejection of ~ 90 % and the lowest adsorbed amount of ~ 85 μg/cm^2, reflecting superior

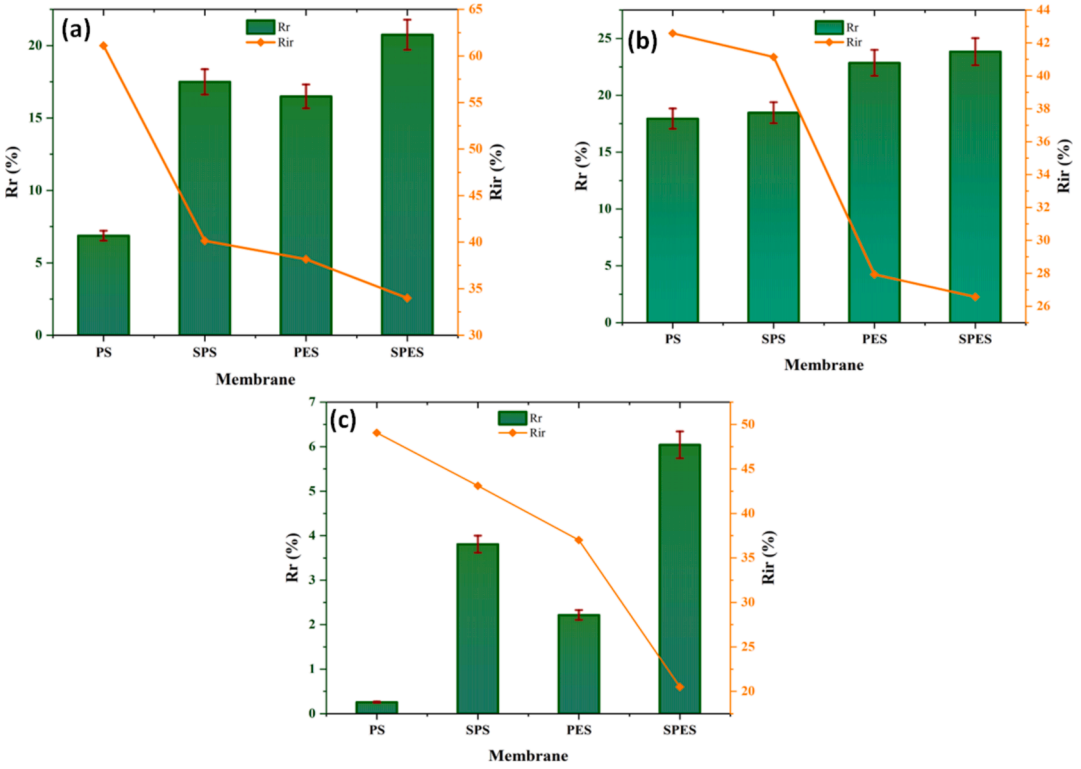

Fig. 8. Fouling resistance (R_r, and R_{ir}) of the neat PES, PS and their sulfonation products (SPES and SPS) membranes using different foulants (a) BSA, (b) HA, and (c) SA.

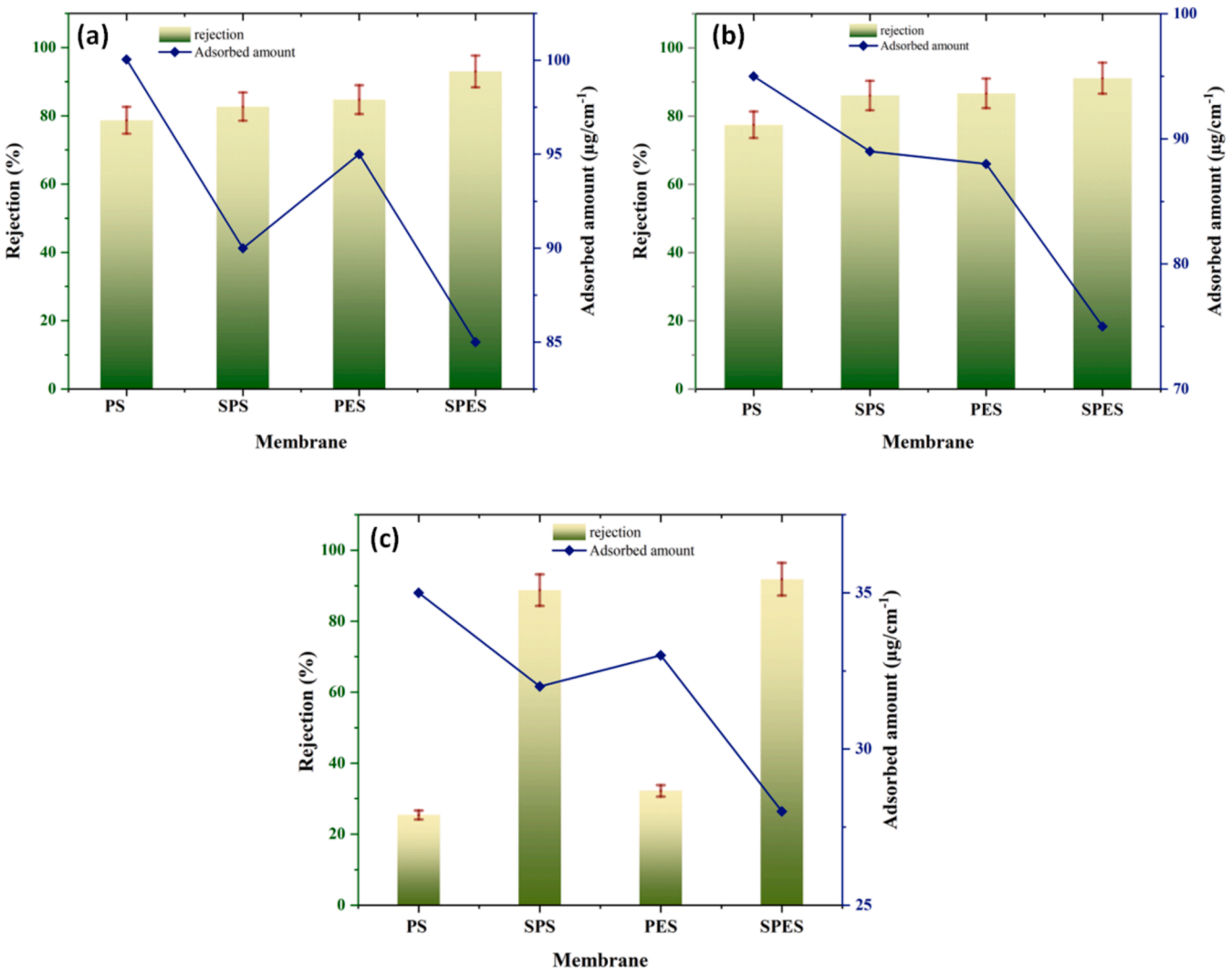

Fig. 9. Rejection assessment and adsorbed quantity of the neat PES, PS and their sulfonation products (SPES and SPS) using various foulants (a) BSA, (b) HA, and (c) SA.

performance due to increased hydrophilicity and reduced fouling. For HA (Fig. 9**b**), the PS membrane shows a rejection of ~ 60 % and an adsorbed amount of ~ 95 μg/cm2. The SPS membrane improves the rejection to ~ 65 %, with a slightly lower adsorbed amount of ~ 93 μg/cm2. The PES membrane has a rejection of ~ 70 % and an adsorbed amount of ~ 90 μg/cm2, while the SPES membrane exhibits the highest rejection of ~ 80 % and the lowest adsorbed amount of ~ 85 μg/cm2. This demonstrates that sulfonation improves the membrane's capability to reject HA and reduces fouling. In Fig. 9**c**, for SA, the PS membrane has the lowest rejection of ~ 30 % and the highest adsorbed amount of ~ 40 μg/cm2, indicating severe fouling. The SPS membrane shows a significant improvement in rejection to ~ 50 %, with a reduced adsorbed amount of ~ 35 μg/cm2. The PES membrane has a rejection of ~ 70 % and an adsorbed amount of ~ 30 μg/cm2, while the SPES membrane exhibits the highest rejection of ~ 80 % and the lowest adsorbed amount of ~ 25 μg/cm2. The results indicate that sulfonation greatly enhances SA's antifouling properties and rejection performance. These findings correlate well with the findings obtained from the XRD, SEM, and contact angle analyses.

4. Conclusion

The incorporation of PES, PS, and their sulfonated forms (SPES and SPS) into hybrid UF membranes significantly improved water flux, antifouling properties, and overall performance. Sulfonation increased hydrophilicity, porosity, and thermal stability, with SPES achieving a higher pure water flux (130 L/m^2·h) compared to PS (100 L/m^2·h). Enhanced rejection rates and antifouling performance were observed, with SPES exhibiting higher flux recovery ratios (85 % vs. 60 % for PS). These results demonstrate that sulfonated membranes offer superior permeability and fouling resistance, making them ideal for advanced wastewater treatment applications.

Declaration of competing interest

The authors declare that they have no known competing financial interests or personal relationships that could have appeared to influence the work reported in this paper.

Acknowledgment

This work was funded by the Deanship of Graduate Studies and Scientific Research at Jouf University under grant No. (DGSSR-2024-02-01045).

Appendix A. Supplementary material

Supplementary data to this article can be found online at https://doi.

org/10.1016/j.jksus.2024.103576.

Data availability

Data will be made available on request.

References

Al Malek, S.A., Abu Seman, M.N., Johnson, D., Hilal, N., 2012. Formation and characterization of polyethersulfone membranes using different concentrations of polyvinylpyrrolidone. Desalination 288, 31–39. https://doi.org/10.1016/j.desal.2011.12.006.

Aldawsari, A.M., Hassan, H.M.A., Alrashidi, A.N., Alsohaimi, I.H., Moustafa, S.M.N., Youssef, H.M., Hamdi, R., Azzam, M.A., 2022. Preparation of PVDF-co-PAAm membrane with a robust antifouling and antibacterial performance by blending with magnetic graphene oxide. J. Environ. Chem. Eng. 10, 108093. https://doi.org/10.1016/j.jece.2022.108093.

Alosaimi, E.H., Hassan, H.M.A., Alsohaimi, I.H., Chen, Q., Melhi, S., Younes, A.A., El-Shwiniy, W.H., 2022. Fabrication of sulfonated polyethersulfone ultrafiltration membranes with an excellent antifouling performance by impregnating with polysulfopropyl acrylate-coated ZnO nanoparticles. Environ. Technol. Innov. 25, 102210. https://doi.org/10.1016/j.eti.2021.102210.

Alshahrani, A.A., El-Habeeb, A.A., Alotaibi, N.H., Shaman, A.A., Almutairi, W.F., Alotaibi, S.M., Hassan, H.M., Alsohaimi, I.H., 2022. Preparation and characterization of modified polysulfone with crosslinked chitosan–glutaraldehyde MWCNT nanofiltration membranes, and evaluation of their capability for salt rejection. Polymers (basel). https://doi.org/10.3390/polym14245463.

Alsohaimi, I.H., Alrashidi, A.N., Hassan, H.M.A., Chen, Q., 2023. Highly efficient ultrafiltration membrane performance of PES@microcrystalline cellulose extracted from waste fruits for the removal of BrO3− from drinking water samples. Colloid Interface Sci. Commun. 54, 100718. https://doi.org/10.1016/j.colcom.2023.100718.

Athira, V.B., Mohanty, S., Nayak, S.K., 2020. Preparation and characterization of porous polyethersulfone (PES) membranes with improved biocompatibility by blending sulfonated polyethersulfone (SPES) and cellulose acetate (CA) – A comparative study. Mater. TodayCommun. 25, 101544. https://doi.org/10.1016/j.mtcomm.2020.101544.

Baker, R.W., 2023. Other membrane processes are in membrane technology and applications. pp. 512–524. Doi: 10.1002/9781119686026.ch15.

Celik Madenli, E., Yanar, N., Choi, H., 2021. Enhanced antibacterial properties and suppressed biofilm growth on multi-walled carbon nanotube (MWCNT) blended polyethersulfone (PES) membranes. J. Environ. Chem. Eng. 9, 104755. https://doi.org/10.1016/j.jece.2020.104755.

Dharupaneedi, S.P., Nataraj, S.K., Nadagouda, M., Reddy, K.R., Shukla, S.S., Aminabhavi, T.M., 2019. Membrane-based separation of potential emerging pollutants. Sep. Purif. Technol. 210, 850–866. https://doi.org/10.1016/j.seppur.2018.09.003.

El-Sayed, M.Y., Alsohaimi, I.H., Alrashidi, A.N., Aldawsari, A.M., Alshahrani, A.A., Hassan, H.M.A., 2023. Mixed matrix membrane comprising functionalized sulfonated activated carbon from tea waste biomass for enhanced hydrophilicity and antifouling properties. Diam. Relat. Mater. 136, 109945. https://doi.org/10.1016/j.diamond.2023.109945.

Fang, L.-F., Yang, H.-Y., Cheng, L., Kato, N., Jeon, S., Takagi, R., Matsuyama, H., 2017. Effect of molecular weight of sulfonated poly(ether sulfone) (SPES) on the mechanical strength and antifouling properties of Poly(ether sulfone)/SPES blend membranes. Ind. Eng. Chem. Res. 56, 11302–11311. https://doi.org/10.1021/acs.iecr.7b02996.

Guo, J., Kim, J., 2017. Modifications of polyethersulfone membrane by doping sulfated-TiO2 nanoparticles for improving antifouling property in wastewater treatment. RSC Adv. 7, 33822–33828. https://doi.org/10.1039/C7RA06406C.

Ho, C.-C., Su, J.F., 2022. Boosting permeation and separation characteristics of polyethersulfone ultrafiltration membranes by structure modification via dual-PVP pore formers. Polymer (guildf) 241, 124560. https://doi.org/10.1016/j.polymer.2022.124560.

Kheirieh, S., Asghari, M., Afsari, M., 2018. Application and modification of polysulfone membranes. Rev. Chem. Eng. 34, 657–693. https://doi.org/10.1515/revce-2017-0011.

Khorsand-Ghayeni, M., Barzin, J., Zandi, M., Kowsari, M., 2017. Fabrication of asymmetric and symmetric membranes based on PES/PEG/DMAc. Polym. Bull. 74, 2081–2097. https://doi.org/10.1007/s00289-016-1823-z.

Kochkodan, V., Tsarenko, S., Potapchenko, N., Kosinova, V., Goncharuk, V., 2008. Adhesion of microorganisms to polymer membranes: a photobactericidal effect of surface treatment with TiO2. Desalination 220, 380–385. https://doi.org/10.1016/j.desal.2007.01.042.

Liu, B., Robertson, G.P., Kim, D.-S., Sun, X., Jiang, Z., Guiver, M.D., 2010. Enhanced thermo-oxidative stability of sulfophenylated poly(ether sulfone)s. Polymer (guildf) 51, 403–413. https://doi.org/10.1016/j.polymer.2009.12.014.

Ma, X., Su, Y., Sun, Q., Wang, Y., Jiang, Z., 2007. Enhancing the antifouling property of polyethersulfone ultrafiltration membranes through surface adsorption-crosslinking of poly(vinyl alcohol). J. Memb. Sci. 300, 71–78. https://doi.org/10.1016/j.memsci.2007.05.008.

Mannan, H.A., Mukhtar, H., Murugesan, T., 2015. Preparation and Characterization of Newly Developed Polysulfone/Polyethersulfone Blend Membrane for CO2 Separation. Appl. Mech. Mater. 699, 325–330. https://doi.org/10.4028/www.scientific.net/AMM.699.325.

Mekonnen, M.M., Hoekstra, A.Y., 2024. Four billion people are facing severe water scarcity. Sci. Adv. 2. https://doi.org/10.1126/sciadv.1500323 e1500323.

Myat, D.T., Stewart, M.B., Mergen, M., Zhao, O., Orbell, J.D., Gray, S., 2014. Experimental and computational investigations of the interactions between model organic compounds and subsequent membrane fouling. Water Res. 48, 108–118. https://doi.org/10.1016/j.watres.2013.09.020.

Pereira, V.R., Isloor, A.M., Bhat, U.K., Ismail, A.F., Obaid, A., Fun, H.-K., 2015. Preparation and performance studies of polysulfone-sulfated nano-titania (S-TiO2) nanofiltration membranes for dye removal. RSC Adv. 5, 53874–53885. https://doi.org/10.1039/C5RA07994B.

Rahimpour, A., Madaeni, S.S., Ghorbani, S., Shockravi, A., Mansourpanah, Y., 2010. The influence of sulfonated polyethersulfone (SPES) on surface nano-morphology and performance of polyethersulfone (PES) membrane. Appl. Surf. Sci. 256, 1825–1831. https://doi.org/10.1016/j.apsusc.2009.10.014.

Sadare, O.O., Daramola, M.O., 2021. Blended polysulfone/polyethersulfone (PSF/PES) membrane with enhanced antifouling property for separation of succinate from organic acids from fermentation broth. ACS Sustain. Chem. Eng. 9, 13068–13083. https://doi.org/10.1021/acssuschemeng.1c05059.

Serbanescu, O.S., Voicu, S.I., Thakur, V.K., 2020. Polysulfone functionalized membranes: Properties and challenges. Mater. TodayChem 17, 100302. https://doi.org/10.1016/j.mtchem.2020.100302.

Shannon, M.A., Bohn, P.W., Elimelech, M., Georgiadis, J.G., Mariñas, B.J., Mayes, A.M., 2008. Science and technology for water purification in the coming decades. Nature 452, 301–310. https://doi.org/10.1038/nature06599.

Shen, J., Ruan, H., Wu, L., Gao, C., 2011. Preparation and characterization of PES–SiO2 organic-inorganic composite ultrafiltration membrane for raw water pretreatment. Chem. Eng. J. 168, 1272–1278. https://doi.org/10.1016/j.cej.2011.02.039.

Shi, X., Tal, G., Hankins, N.P., Gitis, V., 2014. Fouling and cleaning of ultrafiltration membranes: A review. J. Water Process Eng. 1, 121–138. https://doi.org/10.1016/j.jwpe.2014.04.003.

Van der Bruggen, B., 2009. Chemical modification of polyethersulfone nanofiltration membranes: A review. J. Appl. Polym. Sci. 114, 630–642. https://doi.org/10.1002/app.30578.

Venault, A., Liou, C.-S., Yeh, L.-C., Jhong, J.-F., Huang, J., Chang, Y., 2017. Turning Expanded Poly(tetrafluoroethylene) Membranes into Potential Skin Wound Dressings by Grafting a Bioinert Epoxylated PEGMA Copolymer. ACS Biomater. Sci. Eng. 3, 3338–3350. https://doi.org/10.1021/acsbiomaterials.7b00732.

Wang, J., Qiu, M., He, C., 2020. A zwitterionic polymer/PES membrane for enhanced antifouling performance and promoting hemocompatibility. J. Memb. Sci. 606, 118119. https://doi.org/10.1016/j.memsci.2020.118119.

Wang, Y.-H., Wu, Y.-H., Tong, X., Yu, T., Peng, L., Bai, Y., Zhao, X.-H., Huo, Z.-Y., Ikuno, N., Hu, H.-Y., 2019. Chlorine disinfection significantly aggravated the biofouling of reverse osmosis membranes used for municipal wastewater reclamation. Water Res. 154, 246–257. https://doi.org/10.1016/j.watres.2019.02.008.

Wu, H.-L., Ma, C.-C.-M., Liu, F.-Y., Chen, C.-Y., Lee, S.-J., Chiang, C.-L., 2006. Preparation and characterization of poly(ether sulfone)/sulfonated poly(ether ether ketone) blend membranes. Eur. Polym. J. 42, 1688–1695. https://doi.org/10.1016/j.eurpolymj.2006.01.018.

Yi, Z., Zhu, L., Cheng, L., Zhu, B., Xu, Y., 2012. A readily modified polyethersulfone with amino-substituted groups: Its amphiphilic copolymer synthesis and membrane application. Polymer (guildf) 53, 350–358. https://doi.org/10.1016/j.polymer.2011.11.053.

Zhang, S., Cao, J., Ma, N., You, M., Wang, X., Meng, J., 2018. Fast and facile fabrication of antifouling and hemocompatible PVDF membrane-tethered with amino-acid modified PEG film. Appl. Surf. Sci. 428, 41–53. https://doi.org/10.1016/j.apsusc.2017.09.112.

Zhang, M., Ni, F., He, J., Liu, Y., 2021. Evaluation of the formation and antifouling properties of a novel adsorptive homogeneous mixed matrix membrane with in situ generated Zr-based nanoparticles. RSC Adv. 11, 8491–8504. https://doi.org/10.1039/D0RA10330F.

Zhao, F., Xu, K., Ren, H., Ding, L., Geng, J., Zhang, Y., 2015. Combined effects of organic matter and calcium on biofouling of nanofiltration membranes. J. Memb. Sci. 486, 177–188. https://doi.org/10.1016/j.memsci.2015.03.032.

Zhao, C., Xue, J., Ran, F., Sun, S., 2013. Modification of polyethersulfone membranes – A review of methods. Prog. Mater. Sci. 58, 76–150. https://doi.org/10.1016/j.pmatsci.2012.07.002.